Theor Chem Acc (2016) 135:71
DOI 10.1007/s00214-016-1828-6

REGULAR ARTICLE

Studying the binding mechanisms of veratryl alcohol to *P. chrysosporium* lignin peroxidase: insights from theoretical approaches

Rodrigo Recabarren[1] · Isabel Fuenzalida-Valdivia[1] · Jans Alzate-Morales[1]

Received: 15 October 2015 / Accepted: 3 February 2016 / Published online: 1 March 2016

Abstract Veratryl alcohol (VA) is the main substrate of lignin peroxidase (LiP), a key lignin-degrading enzyme. A redox mediator role, in the lignin degradation process, has been attributed to this molecule; however, many unanswered questions remain about its action mechanism. In this investigation, the basic aspects of a plausible action mechanism, this means VA binding modes to *Phanerochaete chrysosporium* LiP, were addressed. Docking calculations were used to obtain LiP–VA complexes near to Trp171, the active redox residue where VA is oxidized. Our results show that VA interacts at Trp171 helped by hydrogen bonding interactions with the acidic amino acids Asp264 and Glu168, as well as by hydrophobic interactions with Phe267, confirming previous experimental findings. MM–GBSA calculations, molecular dynamics simulations, and cluster analysis gave further insights into the energetic preferences of the different binding modes and the stability of LiP–VA complexes. A hydrophobic concave ditch, next to Trp171, was observed to stabilize VA at LiP surface, confirming previous suggestions based on the LiP crystal structure. A detailed analysis of the interactions in this site is provided. These findings are expected to be the basis for site-directed mutagenesis and QM/MM experiments that will prove the importance of the identified residues.

Keywords Lignin-degrading enzymes · LiP · Biotransformations · Molecular dynamics · MM/GBSA · Value-added products

1 Introduction

Lignin is an aromatic polymer present in the cell wall which constitutes the second most abundant natural polymer on earth after cellulose [1]. Lignin possesses a very complex and heterogeneous structure, which makes it highly recalcitrant to biodegradation. Due to this, specific lignolytic enzymes are required to complete its depolymerization and mineralization, step that is crucial in the carbon cycle [2, 3]. Fungal organisms are the main natural machineries that secret specific lignin-degrading enzymes, with the white-rot basidiomycetous fungi having the better performance [4–6]. Among lignolytic enzymes, lignin peroxidase (LiP), a heme-containing peroxidase, plays a key role in the degradation of lignin and a variety of phenolic and nonphenolic lignin-model compounds [7–10]. LiP was first discovered in the basidiomycete *Phanerochaete chrysosporium* [7, 11], and from there on, it has been focus of extensive research aiming at elucidating the mechanisms behind lignin degradation. Despite this, there are many aspects of the LiP-degrading mechanism that remain unclear.

It is well known that LiP undergoes the classical mechanism of peroxidases [12], in which LiP reacts with H_2O_2 to form compound I, which after being reduced by one electron generates compound II, to finally recover the ferric state of the enzyme through an additional single electron

Published as part of the special collection of articles "CHITEL 2015 - Torino - Italy".

Electronic supplementary material The online version of this article (doi:10.1007/s00214-016-1828-6) contains supplementary material, which is available to authorized users.

✉ Jans Alzate-Morales
jalzate@utalca.cl; jalzatemorales@gmail.com

[1] Centro de Bioinformática y Simulación Molecular, Facultad de Ingeniería, Universidad de Talca, 2 Norte 685, Casilla 721, Talca, Chile

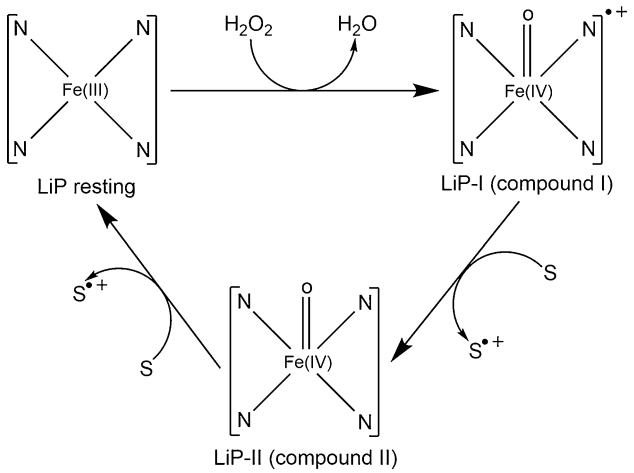

Scheme 1 The catalytic cycle of LiP. The four N atoms stand for the porphyrin ring, and S is an electron-donating substrate. Reaction scheme adapted from Ref. [3]

reduction reaction [3]. The LiP catalytic cycle is resumed in Scheme 1.

Compounds I and II in LiP are oxoferryl species that have the ability to oxidize high redox potential substrates, making the use of LiP and other peroxidases of great interest for scientific, industrial, and biotechnological applications [13–16]. Interestingly, LiP has a higher redox power than other peroxidases, which has been attributed to a longer distance of the proximal His residue to the iron atom at the heme group, what would leave a deficiency of electronic charge over it, enhancing its oxidative power [17].

The first assumption on the LiP-degrading mechanism was to think that lignin units were directly oxidized at the heme group. However, after obtaining the first crystal structures for LiP, it became obvious the impossibility of lignin to approach the heme group [17–19]. The first binding site for substrates was proposed to be located at the entrance of the main access channel, which has been denominated the "classical heme edge" binding site in peroxidases [20, 21]. Computational modeling studies of veratryl alcohol (VA) [22], the main substrate of LiP, showed that the ligand could be accommodated at this pocket and be stabilized by specific hydrogen bonding and hydrophobic interactions [20]. Other computational studies have also predicted that the main access channel would sustain a certain degree of flexibility that would allow the entrance of VA through it to the heme region [23]. However, later on, a high-resolution crystal structure of LiP [17] revealed that Trp171, a solvent-exposed residue, was hydroxylated at its Cβ, giving therefore new insights for a different binding site [24]. Site-directed mutagenesis experiments have confirmed that the presence of Trp171 is imperative for the oxidation of VA as well as for other lignin-model compounds [25–28]. This fact helped to reach the consensus that the mechanism behind LiP activity is a long-range electron transfer (LRET) reaction from the surface of the protein to the heme group. On the other hand, it has been seen that mutation of Trp171 does not abolish the oxidation of other negatively charged substrates, reaching the conclusion that more than one binding site in LiP should exist, with important evidence that the "classical heme edge" binding site should be one of them [25].

VA is the preferred substrate of LiP which has shown to be crucial for avoiding enzyme inactivation [9]. VA is secreted in vivo by the fungus *P. chrysosporium* and therefore is present in the degradation process of lignin. To this molecule has also been attached the role of redox mediator [29, 30]. VA, after being oxidized to a radical cation species ($VA^{\cdot+}$) by Trp171, could work as a diffusible oxidant through the lignin matrix initiating a cascade of radical reactions in polymeric lignin [31, 32]. On the other hand, other authors have proposed the idea that once $VA^{\cdot+}$ is generated, it is held at the protein surface by electrostatic forces where it could work as a redox mediator [33, 34]. These two hypotheses have been introduced in terms of measurements of the lifetime of the $VA^{\cdot+}$ species; however, rather controversial results have been obtained so far. It has also been demonstrated that the presence of VA in the medium is not necessary for the catalytic activity of LiP. The latter is able to oxidize different lignin-model compounds driving their depolymerization by a direct interaction with them without the intervention of redox mediators [28, 35, 36]. However, the presence of VA has shown to increase LiP-degrading activity toward different types of substrates [37–40].

Within this context, not much experimental and theoretical work has been done to identify crucial interactions for VA binding and to explore the specific mechanisms through which VA is stabilized at LiP surface. Sollewijn Gelpke et al. [27] studied the effect of single mutations on residues at different locations on LiP. Mutations of residues near the main access channel confirmed that they were not involved in neither VA oxidation nor in its binding to LiP. On the other hand, mutation of Trp171 completely abolished VA oxidation. Mutation of Phe267, a nearby residue to Trp171, did slightly change VA oxidation levels but more notably its binding to LiP. Therefore, the authors proposed the involvement of Phe267 in the binding of VA at the surface of LiP through the formation of π-stacking complexes. On the other hand, the most clarifying results have been given by Smith and Doyle [41], where they performed single mutations of the near acidic residues to Trp171, which revealed that modifications of Glu168, Glu250 and Asp165 strongly affect the binding (K_m) and oxidation (V_{max}) of VA, while mutation of Asp264 does not have an apparent effect on LiP activity. In particular, mutation of Glu168 has

the strongest impact on the kinetics effectiveness (7 times less effective than wild-type LiP), presuming that this residue could be involved in the stabilization of the postulated complex [Trp171–VA]$^{\cdot+}$.

Among other theoretical studies, Francesca Gerini et al. [23] used steered molecular dynamics simulations to explore the binding process of VA to the heme group, where it was postulated that VA could approach the active site through the main access channel. However, the binding process at Trp171 was not considered. Recently, Chen et al. [42] performed molecular docking calculations and molecular dynamics simulations to analyze the binding modes of a lignin-model molecule at the active site of LiP and other lignolytic enzymes. Although valuable information on interactions that stabilize lignin at the active site of LiP was identified, the binding of lignin at Trp171 was also not explored. More recently, Miki et al. [43] discovered a novel oxidation mechanism for *Trametopsis cervina* LiP, where they observed that the active redox residue Tyr181 forms an adduct with VA which is fundamental for the catalytic activity of LiP. It was seen by means of docking and molecular dynamics calculations that VA is stabilized at Tyr181 by sandwich π-stacking interactions involving Phe89. It is worth noting that Tyr181 from *T. cervina* is located at a different position compared to Trp171 from *P. chrysosporium*. Tyr181 is adjacent to one of the propionate group, what would be the "front side" of LiP close to the access channel, while Trp171 is located at the "back side" of the enzyme [17, 44]. However, it could be expected that similar interactions govern the stabilization of VA at LiP surface since both redox residues are surrounded by mostly acidic amino acids and aromatics such as Phe [44, 45].

The exact nature of the Trp171 radical has also been object of study [46, 47]. After the LRET reaction to the heme has taken place, Trp171 would form the tryptophanyl radical cation (Trp171$^{\cdot+}$) [48]; however, evidence for it has not been obtained so far, but instead, only the Trp171$^{\cdot}$ radical has been detected in LiP variants [46]. The hypothesis that Trp171$^{\cdot+}$ may exist is supported by the existence of the acidic residues around Trp171 that would help to stabilize Trp171$^{\cdot+}$. Quantum mechanics/molecular mechanics (QM/MM) calculations have predicted that deprotonation of Trp171$^{\cdot+}$ is energetically unfavorable and that detection of Trp171$^{\cdot+}$ could have not been achieved most likely due to its very short half-life [47].

The present investigation is therefore focused on elucidating the main interactions of VA at the *P. chrysosporium* LiP surface and to study the mechanisms by which VA is stabilized on it. Even though site-directed mutagenesis experiments have revealed the importance of different residues at the vicinity of Trp171, there are no computational studies, to the best of our knowledge, that may offer atomistic details about the interactions of VA at Trp171 and its main binding modes. For instance, several aspects of the binding process of VA will be addressed such as: Is VA stabilized at the surroundings of Trp171? What are the main binding modes for VA at Trp171? What is the role of Phe267, Glu168, and the other acidic amino acids in VA binding? Are there other key residues for VA stabilization at the vicinity of Trp171? To answer these questions, molecular docking calculations together with MD and binding free energy (ΔG) simulations will be used to analyze the dynamical behavior of LiP–VA complexes.

2 Methods

2.1 Docking, MM–GBSA calculations, and MD simulations

The crystal structure of *P. chrysosporium* LiP (PDB ID: 1LLP [17]) was taken from the protein data bank [49]. The protein structure was processed using the *Protein Preparation Wizard* tool from Maestro [50–52]. Assignment of bond orders, addition of hydrogen atoms, and correction of bad contacts were also carried out with this tool. The four carbohydrate molecules were deleted following the protocol given in previous studies [23]. We expect that this modification will have a minimum impact on our simulations since the unglycosylated enzyme exhibits identical properties than the wild type (WT) [53]. Subsequently, protonation states and hydrogen bond networks were optimized at a pH of 4.5 using the Propka program [54]. This value of pH was chosen since LiP presents its optimal degrading activity at low pHs [48]. Titratable residues were carefully inspected considering their direct microenvironment. Specially, residues Glu168 and Asp264, which were protonated by Propka, were kept deprotonated since it has been postulated they would participate in stabilizing the tryptophanyl radical. Afterward, the protein structure was submitted to a restrained minimization up to a RMSD (root-mean-square deviation) convergence criterion of 0.3 Å. VA was docked in the resulting structure using the Glide software [55–57]. Standard and extra precision settings were applied generating a final set of 20 poses. The grid box was centered on Trp171, and dimensions were set to 20 × 20 × 20 Å. The rest of the specifications were maintained as default. Parameters for LiP and VA were taken from the OPLS-2005 force field [58].

Molecular dynamics simulations were performed with the software Desmond [59]. The 20 docking poses served as starting conformations for our MD simulations. In each case, the system was inserted in an orthorhombic box of SPC [60] water molecules and neutralization was achieved by addition of 5 Na^+ ions. A buffer of 10 Å was imposed over all sides of the protein surface. Periodic boundary

conditions were set over the *x*, *y,* and *z* axes. The default relaxation protocol implemented in Desmond 3.4 was used. Briefly, this protocol consists in six steps in which the system is firstly energy minimized using a steepest descent algorithm switching on and switching off restraints over heavy atoms. Then, four short (12 and 24 ps) MD simulations are performed retaining restraints to finally perform an unrestrained simulation. MD simulations were run in a NPT ensemble keeping the temperature at 300 K by means of the Nosé–Hoover chain method [61] with a relaxation time of 1 ps. Pressure was kept fixed at 1 atm. using the Martyna–Tobias–Klein (MTK) barostat [62] with a relaxation time of 2 ps. A cutoff radius of 9 Å was used for van der Waals as well as electrostatic interactions. For the treatment of long-range electrostatic interactions, the particle mesh Ewald method [63] was considered. The RESPA (time-reversible reference system propagator algorithm) integrator [64] was used, and a time step of 2 fs was set for bonded and short-range nonbonded interactions, while for long-range electrostatics 6 fs was used.

Molecular mechanics/generalized Born surface area (MM–GBSA) calculations were performed with the program Prime [65, 66]. In one case, input structures were taken from docking calculations and in a second case representative structures from MD simulations were used. In either case, the ligand strain energy was considered, but entropic contributions to the binding energy were not. However, we expect the latter assumption to have little impact on our analysis since we are interested in relative binding energies of the same ligand and receptor; therefore, inclusion of entropic contributions should not alter the general trend for binding energies. On the other hand, Prime uses the VSGB 2.0 solvation model [67], which incorporates novel physics-based corrections to the energy function for the description of hydrogen bonding, hydrophobic, and π-stacking interactions. Furthermore, this approach contains a residue-dependent dielectric protocol that has proved to provide adequate estimations of protein–ligand binding energies [68, 69].

2.2 VA, Trp171, and heme parameters

Parameters for VA, Trp171, and the oxoferryl heme group were extracted from the OPLS-2005 force field (see Fig. S1 from Supplementary Information). The quality of these parameters was tested by single-point calculations with the software MacroModel [70] resulting in high-quality parameters, and only medium-quality parameters were found for torsional angles of the heme group. The calculated RMSDs for the oxoferryl group and backbone atoms (Fig. S2) show a quick stabilization of the protein and the heme group confirming the suitability of the used parameters. Furthermore, these parameters and the charges for VA were compared with those used in previous theoretical studies [23, 47] finding good agreement with them in terms of sign and magnitude of the charges.

2.3 Cluster analysis

Clustering was carried out by a hierarchical average-linkage method [71] as implemented in Maestro [50], through the script *trajectory_cluster.py*. We used this method based on previous studies where this algorithm has been applied showing successful results [72, 73]. The residues used to build the RMSD distance matrix were Phe267, Trp171, and the VA ligand. Molecular dynamics simulations of VA close to Trp171 were used for clustering. Here, only frames in which the distance between VA centroid was within a range of 7.5 Å to the Trp171 centroid were considered. This cutoff radius was chosen after analyzing single-point QM/MM (quantum mechanics/molecular mechanics) calculations in which VA and Trp171 were gradually separated and the spin density distribution was evaluated. It was seen that after 7.5 Å the spin density distribution was not shared between VA and Trp171, but it was only localized on Trp171 (Fig. S3). Therefore, this cutoff radius is a good estimate of the longest distance between these two fragments that may favor the formation of the $VA^{\cdot+}$ species (see Supp. Information). As a result, 5503 frames were analyzed from which 5 clusters were extracted. Other numbers of clusters were also evaluated, but it was observed that more than 5 clusters yielded clusters with very low populations and with conformations already replicated in other groups. Representatives were selected based on the structure contained in a cluster closest to the centroid of that group.

3 Results and discussions

3.1 Docking studies

Docking calculations are the preferred computational technique for obtaining energy-minimized complexes for the study of protein–ligand interactions. For this reason, docking studies were performed with the aim of finding the most favorable conformations for VA binding at Trp171. Figure 1a shows that docking experiments predict the formation of two clusters, one with VA roughly lying below the plane of Trp171 (cluster 1) and other above its plane (cluster 2). In the former, the most relevant interactions are hydrogen bonds with Asp264 and π-stacking interactions with Phe267. Within this cluster, poses mostly differ in the orientation of VA with respect to Phe267, with VA being in some cases in a face-to-face geometry (Fig. 1b) and in other cases in an edge-to-face geometry (Fig. 1c). The second cluster is mainly made up by structures forming

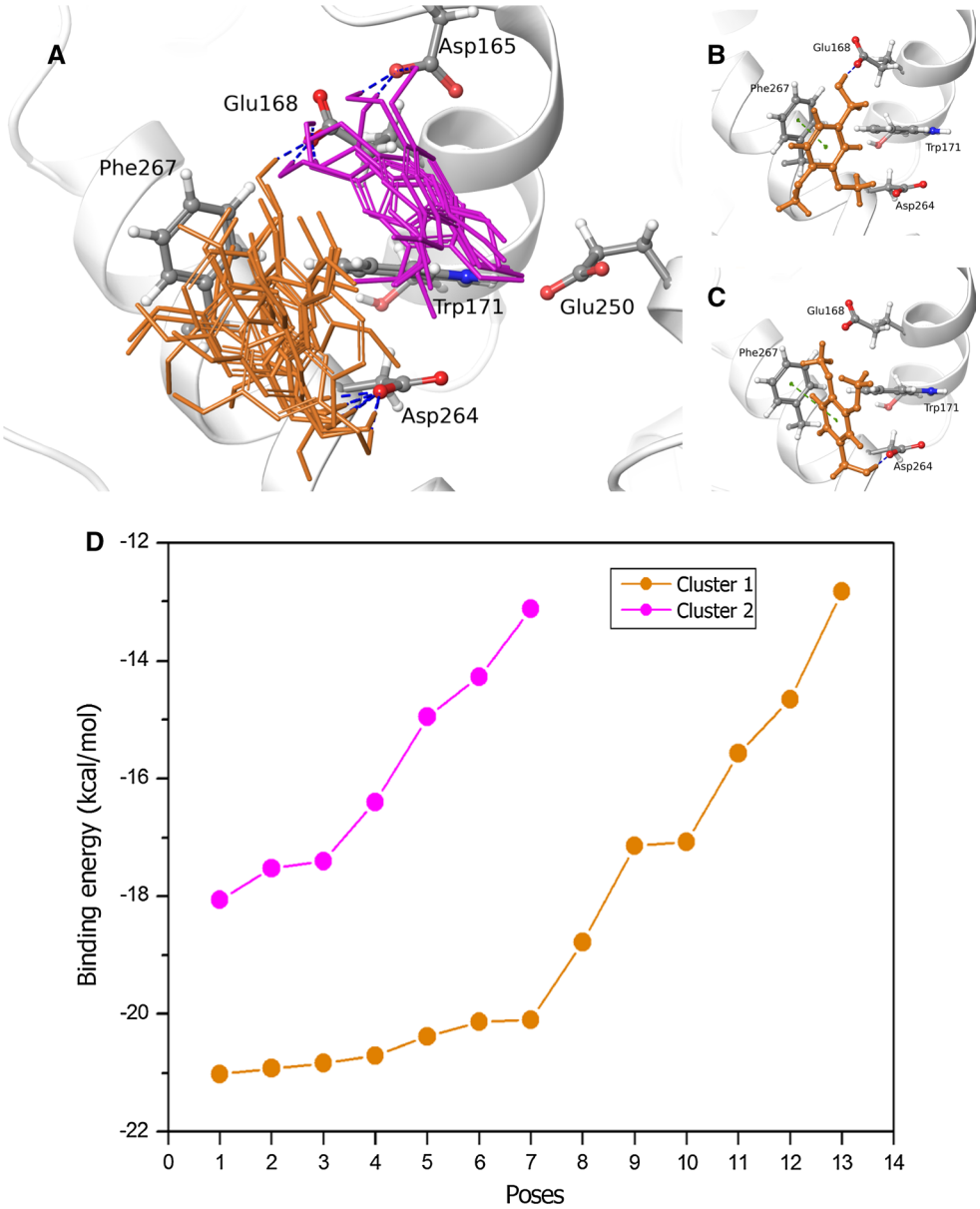

Fig. 1 **a** Poses from docking calculation of VA at Trp171 showing the formation of two clusters: cluster 1 (*orange*) and cluster 2 (*purple*). Hydrogen bonds are represented as *dashed blue lines*. **b** One docking pose showing a face-to-face π-stacking interaction between VA and Phe267, represented as a *dashed green line*. **c** One docking pose showing an edge-to-face π-stacking interaction between VA and Phe267, represented as a *dashed green line*. **d** Binding free energies for the 20 docking poses sorted by those belonging to cluster 1 (*orange*) and cluster 2 (*purple*)

hydrogen bonds with Glu168 and Asp165, with VA being in an inclined orientation with respect to the plane of Trp171. For each docking pose, the ΔG was estimated by the MM–GBSA approach. Figure 1d shows the ΔG values for poses of clusters 1 and 2. From the 20 docking structures, 13 of them belong to cluster 1 and 7 to cluster 2. Figure 1d clearly shows that the structures of cluster 1 exhibit a lower binding energy than the structures of cluster 2, especially for the seven lowest energy poses. The average ΔG values for clusters 1 and 2 are -18.47 and -15.96 kcal/mol, respectively, and the average ΔG values for the seven lowest energy poses in cluster 1 is -20.58 kcal/mol, evidencing a considerable difference of 4.6 kcal/mol with the average ΔG values of cluster 2 (Table 1). In order to elucidate the role of Phe267 in VA binding, the Phe267Ala mutant was prepared and new docking calculations were performed (Fig. S4). Table 1 displays the predicted ΔG values alongside with some energy contributions to it for the seven lowest energy structures of cluster 1, cluster 2, and the mutant Phe267Ala. It results clearly from Table 1 that the energetic preference of structures belonging to cluster 1 is due to the closeness of Phe267 to VA with which it can form hydrophobic and π-stacking interactions. This is evidenced by an enhanced energy contribution from these two types of interactions (ΔE_{lipo} and $\Delta E_{\text{packing}}$, respectively) in this cluster with respect to cluster 2 and the Phe267Ala mutant. In these latter two, VA does not form π-stacking interactions ($\Delta E_{\text{packing}} = 0$) and hydrophobic contributions are very similar between both (-8.55 and -8.48 kcal/mol, respectively). The rest of the energy terms

Table 1 Averaged binding free energies predicted by the MM–GBSA approach

	ΔE^{a}_{elec}	ΔE^{b}_{vdw}	ΔE^{c}_{solv}	$\Delta E^{d}_{packing}$	ΔE^{e}_{lipo}	ΔG^{f}_{pred}
Cluster 1	-6.05 ± 2.38^{g}	-12.20 ± 0.55	9.43 ± 1.39	-1.47 ± 1.04	-10.21 ± 0.78	-20.58 ± 0.35
Cluster 2	-5.61 ± 1.81	-12.73 ± 0.65	11.06 ± 2.96	0.00	-8.55 ± 0.21	-15.96 ± 1.87
Phe267Ala mutant	-5.38 ± 0.77	-11.73 ± 0.66	8.23 ± 1.03	0.00	-8.48 ± 0.05	-16.35 ± 0.69

Seven lowest energy docking poses from cluster 1, cluster 2, and Phe267Ala mutant were selected to perform the calculations. The most important calculated energy components to ΔG_{pred} were [a] electrostatic energy, [b] van der Waals energy, [c] solvation energy, [d] packing energy accounting for ligand–protein π-stacking interactions, [e] lipophilic energy accounting for ligand–protein hydrophobic interactions, and [f] predicted binding free energy. [g] Standard deviation is shown beside each averaged energy value

are approximately similar for the three groups of structures; however, in some cases, high variations are seen, e.g., ΔE_{elec} and ΔE_{solv}, due to the small data set used. Figure 1b, c shows two representative docking poses from cluster 1 where VA forms face-to-face and edge-to-face π-stacking interactions with Phe267.

At first, these results show that VA is more stabilized in a conformation given by cluster 1 than one given by cluster 2. However, Phe267 is expected to attain some degree of flexibility, and therefore, dynamical contributions to these interactions should be taken into account, point that is addressed below.

3.2 MD simulations and interaction profiles

As was explained in the Sect. 1, it is not clear yet whether VA fulfills its redox mediator role as a diffusible oxidant or acts from the protein surface. Since Trp171 is a solvent-exposed residue, it is plausible to think that specific amino acids should be required to achieve proper stabilization of VA at the protein surface, in its either neutral or radical cation form. For this purpose, molecular dynamics simulations were used to assess the permanency of VA at the vicinity of Trp171 and to identify crucial interactions for its binding. The bound state of VA was analyzed by monitoring the distances between the centroids of VA and Trp171, results shown in Fig. 2. Here, six simulations were chosen by simply visual inspection to depict the general behavior of the 20 simulations. It is possible to see a heterogeneous stabilization pattern of VA to the LiP surface at Trp171 where in two cases (poses 1 and 2) VA remains close to Trp171 after 3 ns of simulation, while in the rest of the cases VA escapes to the solvent at different time frames. In general, in 50 % of the simulations, i.e., 10 out of 20, VA does not go to the solvent, remaining close to Trp171 interacting with different residues within an approximate radius of 9 Å.

The 10 simulations in which VA stuck around at the LiP surface were used to identify the most important interactions for VA binding. For this purpose, only frames where VA remained within a cutoff radius of 9 Å with respect to the centroid of Trp171's benzene ring were analyzed.

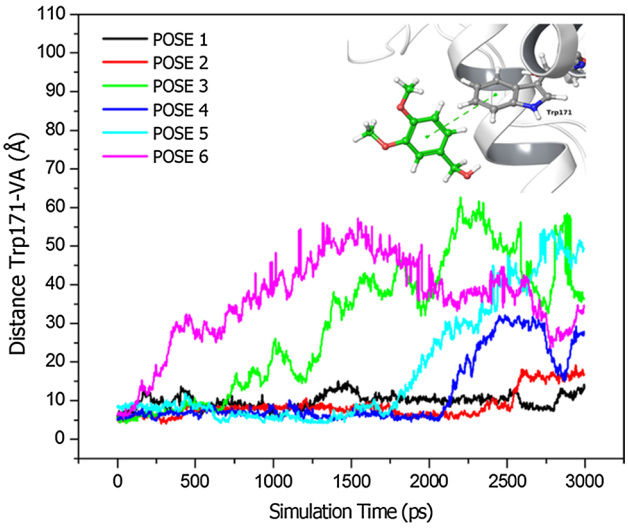

Fig. 2 Centroid–centroid distances between VA and Trp171 for 6 selected MD simulations (the *inset* shows an example of the centroid–centroid measurement)

Several frames were collected making a total simulation of 26.4 ns. The percentage of duration of the identified interactions was estimated by using the *Simulation Interactions Diagram* (*SID*) built-in tool implemented in Maestro [50]. Figure 3 displays the most relevant interactions and how long these interactions lasted during the course of the combined simulation.

It results clear that hydrophobic interactions with Phe267 dominate over the simulation period having a total percentage of duration of 59.5 %. This percentage can be further broken down in contributions from general hydrophobic contacts, face-to-face and edge-to-face π-stacking interactions. The highest contribution to hydrophobic interactions comes from pure hydrophobic contacts having a weight of 41.1 %. Some establishment of π-stacking complexes with similar contributions from face-to-face (11.4 %) and edge-to-face (7.0 %) conformations is also seen. The second more important interaction is hydrogen bonding with Asp264, exhibiting a 52.2 % of duration. The total percentage of interaction with Trp171 is of

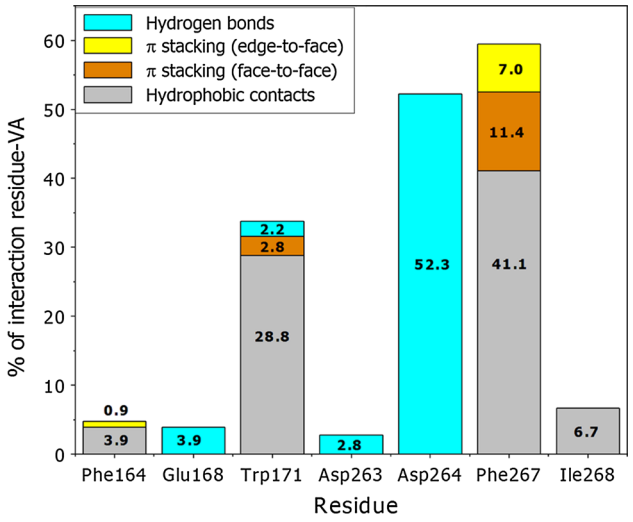

Fig. 3 Interaction profile for a combined MD simulation of 26.4 ns that was generated by combining 10 MD simulations where VA lies within a radius of 9 Å with respect to the Trp171's centroid. The interactions between VA and the residues at the vicinity of Trp171 are rationalized in terms of hydrogen bonds (*cyan*), edge-to-face π-stacking interactions (*yellow*), face-to-face π-stacking interactions (*orange*), and hydrophobic contacts (*gray*). The numbers in bold black inside the bars show the exact percentage of duration of that interaction in the combined MD simulation

33.8 %, showing that VA does not remain attached to this residue very long. Most of the interactions with Trp171 correspond to hydrophobic contacts with some formation of edge-to-face π-stacking interactions (2.8 %) and hydrogen bonds (2.2 %) involving the hydroxyl group at its Cβ. Very interestingly, hydrogen bonds with Glu168 are very scarce, showing that hydrogen bonding interactions with this residue are not maintained in the simulation. This supports what was observed with docking calculations, where the structures forming hydrogen bonds with Glu168 (cluster 2) had a lower binding energy than structures forming hydrogen bonds with Asp264. It is also noticed that hydrogen bonds with Asp165 are practically undetected. This result could be interpreted as contrary to the experimental finding that Glu168 has a great impact in VA binding [41], but on the other hand it may suggest that this acidic residue is more important for the stabilization of the complex $[Trp171–VA]^{\cdot+}$ than for unoxidized VA. This issue could be addressed by performing MD simulations with a charge distribution that correctly represent the positive charge over VA, or by means of QM/MM MD simulations where a quantum mechanical treatment of the radical could be done. Summarizing, it seems clear the importance of Phe267 and acidic amino acids such as Asp264 in the stabilization of VA at Trp171; however, Trp171–VA complexes are observed only for few nanoseconds.

3.3 Cluster analysis

In order to identify the most visited configurations for "close-distance" Trp171–VA complexes, a cluster analysis was carried out on the previously combined simulation. Since the goal was to identify Trp171–VA complexes where the electron transfer from VA to Trp171 may take place, a shorter distance of 7.5 Å between the centroids of VA and Trp171 was chosen (see Sect. 2.3). Figure 4 displays the five representative structures belonging to each cluster. Herewith, Table 2 shows the population sizes and the percentage of duration for hydrogen bonding interactions within each group.

According to Table 2, cluster 1 is the most populated containing 54.69 % of the analyzed frames. The representative structure (Fig. 4a) of this cluster positions VA between Trp171 and Phe267 after the latter residue has been flipped with respect to the position given by the crystal structure to a location below the plane of Trp171, more less resembling a parallel-displaced π-stacking geometry. It is also shown that the hydroxyl hydrogen atom of VA is close to the carboxylic oxygen atom of Asp264 featuring a hydrogen bonding interaction that is detected in 54.1 % of the analyzed frames (Table 2). The second most populated cluster is cluster 4 with a population size of 36.14 %. The representative geometry exhibits an edge-to-face π-stacking interaction between VA and Phe267 and hydrogen bonding interactions to Asp264 (Fig. 4d). It is noticed from Table 2 that this hydrogen bond is highly stable throughout this cluster having a contribution of 83.4 %. Cluster 2 is the next most populated cluster with a population size of 6.74 %. The representative structure (Fig. 4b) shows VA closer to Glu168 and Phe164 and not featuring specific interactions with the near-by residues. Next cluster, cluster 5, possesses a relatively low population size of 1.53 %, and its representative structure (Fig. 4e) displays a similar arrangement of Phe267 and VA as in cluster 4 but with VA displaced in an edge-to-face geometry with respect to Trp171. In the representative structure, VA does not form a hydrogen bond with Glu168; nonetheless, this interaction is found in the 74.6 % of the frames of this cluster (Table 2). Finally, cluster 3 has the lowest population size (0.88 %) in which VA in its representative snapshot (Fig. 4c) is located toward Phe164 interacting with this residue and Phe267.

Aiming at measuring the strength of the interaction between VA and LiP for each representative structure, ΔG values were calculated by means of the MM–GBSA approach. Unfortunately, a rather poor correlation was found when the population sizes of all five representatives with respect to the free energy of binding were correlated (Fig. S5.A). This could be explained since the two structures that have low population sizes, but high binding

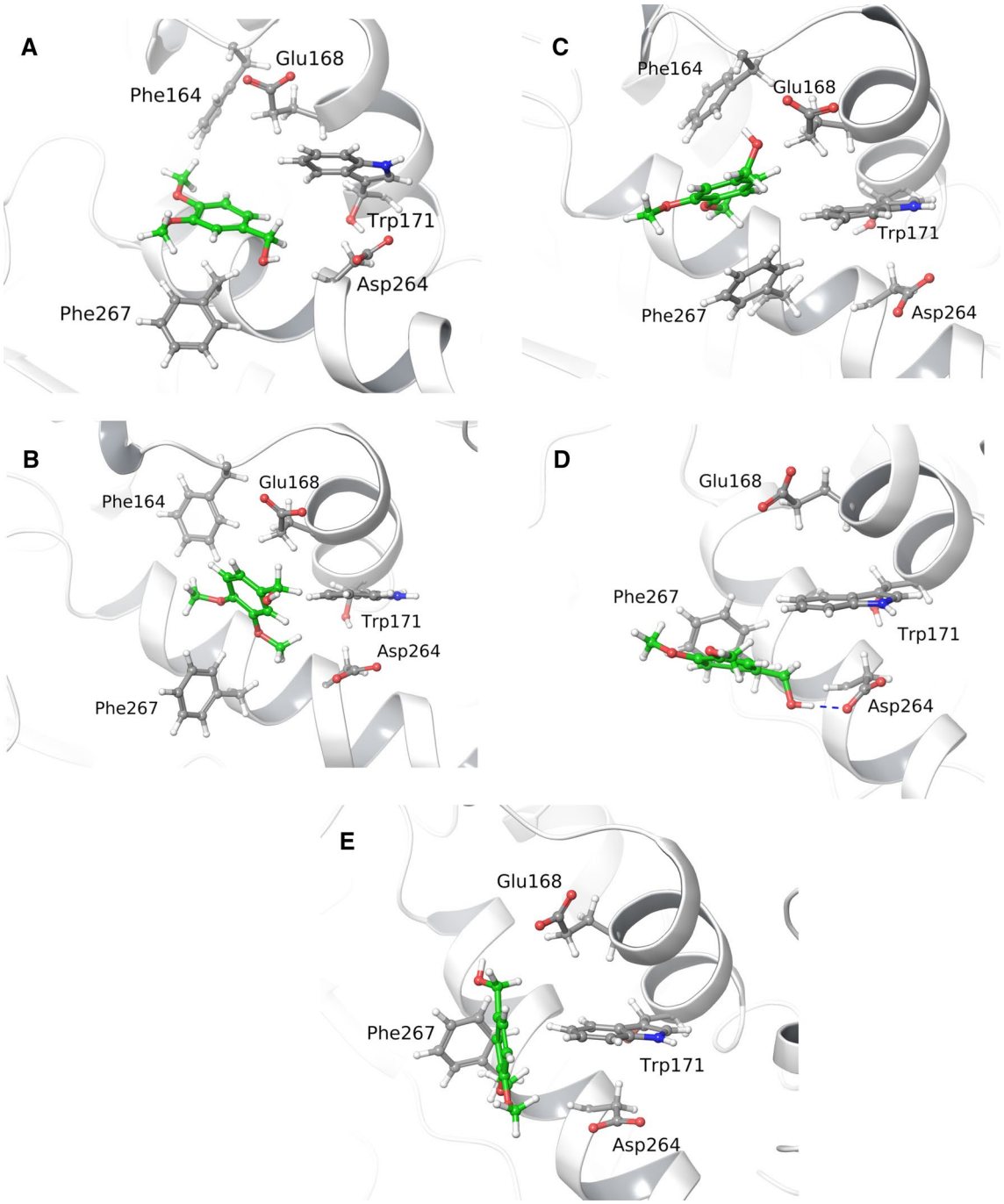

Fig. 4 Representative structures from clustering calculations derived from MD simulations. **a** Representative structure from cluster 1, **b** representative structure from cluster 2, **c** representative structure from cluster 3, **d** representative structure from cluster 4, **e** representative structure from cluster 5. Veratryl alcohol is shown in *green* together with important residues for its binding at Trp171. Hydrogen bonds are represented as *dashed blue lines*

Table 2 Population sizes for each cluster

Cluster	1	2	3	4	5
Population size (%)	54.69 (54.1)	6.74 (11.2*)	0.88 (0.00)	36.14 (83.4)	1.53 (74.6*)

Numbers in parenthesis represent the percentage of duration of hydrogen bonding interactions with either Asp264 or Glu168, the latter distinguished by an asterisk

affinities, correspond to the representatives of clusters 2 and 3 (Fig. 4b, c), where VA approaches a hydrophobic concave ditch close to Phe164 (see Sect. 3 above). For this reason, the population sizes are expected to be small since VA is moving toward that region and the ΔG binding affinities tend to be high. Exclusion of these two structures from the correlation plots renders a Pearson coefficient of −0.99 (Fig. S5.B), while inclusion of all points yields a Pearson coefficient of −0.31 (Fig. S5.A). Within this context, population sizes are considered to be a good parameter to assess the preferred orientations of VA at Trp171.

In conclusion, these results complement the observations already seen in the interaction profiles from Fig. 3. The highly stable hydrogen bonds with Asp264 and π-stacking interactions with Phe267 are clearly rationalized in the structures of the representatives from clusters 1 and 4 (Fig. 1a, d). π-Stacking interactions with Phe267 agree well with experimental findings from Sollewijn Gelpke et al. [27] who found that this residue had an important impact on VA binding. On the other hand, similar results have also been obtained for LiP from *T. cervina* [43], where it was observed that VA forms stable π-stacking complexes with the aromatic residue Phe89 and the active redox residue Tyr181. On the other hand, experimental evidence in *P. chrysosporium* LiP has shown that mutation of Asp264 does affect neither the binding of VA nor the activity of LiP but Glu168 and Asp165 have a pronounced effect on it. As discussed above, this apparent contradiction with our results might be showing that the interaction dynamics of VA and $VA^{\cdot+}$ are substantially different.

3.4 Hydrophobic concave ditch characterization at binding site of LiP

Previous observations of the LiP crystal structure obtained by Choinowski et al. [17] highlighted the existence of a hydrophobic concave ditch next to Trp171 formed by Phe amino acids that could work stabilizing aromatic substrates; however, a detailed characterization of this LiP structural feature was not carried out. This fact led us to consider that this hydrophobic ditch on the protein surface may help to stabilize VA, whether it is in its neutral or radical state. Careful inspection of the 10 MD simulations in which VA did not escape to the solvent revealed that VA in fact approaches this hydrophobic site next to Trp171, where it is highly stabilized. In order to explore the first aspect of this hypothesis, routine MD simulations of VA at this hydrophobic concave ditch were performed. Five out of 10 MD simulations in which VA approached this site were extended to 40 ns for subsequent analysis of important interactions. MD simulations showed that VA remained attached at this hydrophobic ditch for almost all the simulation time in the 5 simulations, except for the case

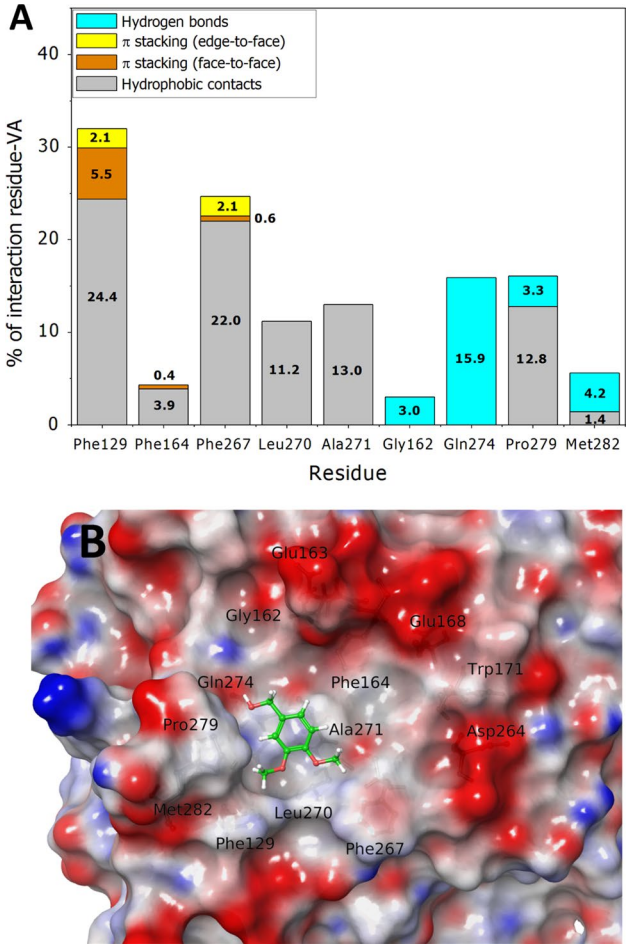

Fig. 5 **a** Interaction profile for a combined MD simulation of 190 ns where VA is stabilized next to Trp171 at a hydrophobic ditch. The interactions between VA and the residues at this site are rationalized in terms of hydrogen bonds (*cyan*), edge-to-face π-stacking interactions (*yellow*), face-to-face π-stacking interactions (*orange*), and hydrophobic contacts (*gray*). The numbers in bold black inside the *bars* show the exact percentage of duration of that interaction in the MD simulation. **b** Snapshot from a 190-ns MD simulation showing VA at the hydrophobic ditch next to Trp171

of two of them where VA exited to the solvent at the last 5 ns. The merging of the 5 trajectories produced a simulation of 190 ns, which was analyzed, and its interaction profiles were generated. Figure 5a shows the main residues that constitute this hydrophobic concave ditch and their contribution to VA binding. The most important residue for VA stabilization was Phe129, with which VA remained interacting during 32 % of the simulation, showing contributions from pure hydrophobic contacts (24.4 %), face-to-face (5.5 %), and edge-to-face (2.1 %) π-stacking interactions. Hydrophobic interactions with Phe267 were also very frequent, with a contribution of 24.7 %, with a large majority of pure hydrophobic contacts (22 %). Hydrophobic interactions with Phe164, Leu270, Ala271, and Pro279

were also detected in a range of 4–13 %. Additionally, hydrogen bonds between the methoxyl oxygens of VA and side chain amino hydrogen atoms of Gln274 had also an important contribution in VA binding with a percentage of duration of 15.9 %. Lastly, minor contributions came from hydrogen bonds between the hydroxyl hydrogen atom of VA with the backbone oxygen atoms of Gly162 and Met282. Figure 5b shows VA at this hydrophobic ditch alongside with the most important residues for its stabilization. The electrostatic potential clearly shows the enhanced hydrophobicity of the residues involved in this site, and very interestingly, with a predominance of aromatic residues such as Phe.

The importance of hydrophobic amino acids at the protein surface in other lignin and cellulose degrading enzymes for catalysis is well established [74, 75]. For instance, fungal cellulases possess a specific binding domain with three aromatic residues that lie at the surface of the subunit and control binding affinity toward cellulose [75]. It has been shown that mutations of these amino acids greatly affect the binding ability of the enzyme and its enzymatic activity [74]. In a similar way, we hypothesize that the hydrophobic amino acids forming this hydrophobic concave ditch, which are the aromatics Phe267, Phe129, and Phe164 together with the hydrophobic amino acids Leu270, Ala271, and Pro279, may play an important role in the stabilization of VA at the protein surface.

The relevance of this hydrophobic ditch, which is part of the binding site at Trp171, could also be inferred from new engineered peroxidases, where LiP activity toward VA has been created in *Coprinus cinereus* peroxidase (CIP) [41]. Here, the active redox residue Trp171 together with other two acidic aminoacids (Asp165 and Glu250) was inserted in their respective equivalent positions at the CiP surface, and VA oxidase activity was successfully implemented. However, the engineered enzyme was found to be 500 less efficient than WT LiP. They confirmed that the inclusion of acidic amino acids was important since the mutant containing only the active Trp exhibited a very low activity. Besides, CiP lacks Phe amino acids at the vicinity of the engineered active Trp; therefore, one reason for the large gap in the activities between mutated CiP and WT LiP may be due to the absence of a hydrophobic site which could stabilize VA at the protein surface. It is worth mentioning that all our observations need to be verified by experimental essays where site-directed mutagenesis experiments will be the key to prove the importance of the identified residues on LiP catalytic activity. Ongoing experimental and computational (at QM/MM level) work is being performed in our laboratory in order to test this hypothesis.

4 Conclusions

Phanerochaete chrysosporium LiP has been focus of considerable research during the years due to its attractive features to be used in industrial and biotechnological applications. However, many aspects of the mechanism by which LiP degrades polymeric lignin and other substrates are still obscure. Great advance has been done in elucidating the importance of the redox active residue Trp171, without which LiP lacks activity toward VA and other lignin-model compounds. In this work, we have contributed to study the main interactions by which VA is stabilized at the LiP surface and specifically at the vicinity of Trp171. Docking calculations predicted that the main binding modes of VA at Trp171 involve hydrophobic interactions with Phe267 and hydrogen bonds with Asp264. The importance of other acidic amino acids such as Glu168 and Asp165 was also discussed. MM–GBSA calculations were used to estimate the binding free energies of the different docking poses confirming that Phe267 makes an important contribution to VA binding as had been proposed earlier from experiments [27].

Molecular dynamics simulations allowed us to study the dynamics of Trp171–VA complexes. It was seen that Trp171–VA complexes exhibit a complex and heterogeneous behavior, since in some cases VA escapes rapidly to the solvent, while in others it remains close to Trp171 interacting through hydrophobic interactions with Phe267 and hydrogen bonds with Asp264. Clustering of the MD frames provided five clusters that resembled the most visited configurations for Trp171–VA complexes. The two most populated clusters showed VA forming π-stacking complexes with Trp171 and Phe267 and forming hydrogen bonds with Asp264, showing that these interactions are stable for "close-distance" complexes during the simulation time. It is noteworthy that previous experimental work has shown that Glu168 has the greatest impact on LiP activity toward VA [41], where its contribution could come from either the stabilization of the $Trp171^{\cdot+}$ species or the $[Trp171–VA]^{\cdot+}$ complex [41]. The fact that we do not observe Glu168 being involved in VA binding may be shedding light on the different stabilization mechanisms of VA and the $VA^{\cdot+}$ species. Future computational and experimental work in our laboratory will be focused on answering these questions to further clarify the role of Glu168.

Finally, routine MD simulations allowed us to characterize a hydrophobic concave ditch previously identified in the LiP crystal structure [17]. Our MD simulations show that when VA remains attached to the LiP surface, it approaches this hydrophobic ditch where it is highly stabilized during the simulation time. We suspect that the hydrophobic residues forming this ditch next to Trp171 could function

driving the recognition of aromatic substrates such as VA and very probably lignin polymeric units. Site-directed mutagenesis of the residues forming this site upon VA binding and catalysis should confirm this.

Acknowledgments J.H.A.M. and I.F.V. acknowledge the financial support from project FONDECYT No. 1140618. R.R. acknowledges support from a doctoral fellowship CONICYT-PCHA/Folio 21130949. We thank Prof. Angel Martínez, from Centro de Investigaciones Biológicas (CIB), Madrid, Spain, for his help in the revision and valuable comments on the first draft of the manuscript.

References

1. Heitner C, Dimmel D, Schmidt J (2011) Lignin and lignans: advances in chemistry. CRC Press, Boca Raton, FL
2. Martínez ÁT et al (2010) Biodegradation of lignocellulosics: microbial, chemical, and enzymatic aspects of the fungal attack of lignin. Int Microbiol 8:195–204
3. Wong DWS (2009) Structure and action mechanism of ligninolytic enzymes. Appl Biochem Biotechnol 157:174–209
4. Kirk TK, Farrell RL (1987) Enzymatic 'combustion': the microbial degradation of lignin. Annu Rev Microbiol 41:465–501
5. Eriksson K-EL, Blanchette RA, Ander P (1990) Microbial and enzymatic degradation of wood and wood components. Springer, Berlin
6. Kersten P, Cullen D (2007) Extracellular oxidative systems of the lignin-degrading Basidiomycete *Phanerochaete chrysosporium*. Fungal Genet Biol 44:77–87
7. Tien M, Kirk TK (1983) Lignin-degrading enzyme from the hymenomycete *Phanerochaete chrysosporium* burds. Science 221:661–663
8. Hammel KE et al (1993) Ligninolysis by a purified lignin peroxidase. J Biol Chem 268:12274–12281
9. Valli K, Wariishi H, Gold MH (1990) Oxidation of monomethoxylated aromatic compounds by lignin peroxidase: role of veratryl alcohol in lignin biodegradation. Biochemistry 29:8535–8539
10. Banci L, Ciofi-Baffoni S, Tien M (1999) Lignin and Mn peroxidase-catalyzed oxidation of phenolic lignin oligomers. Biochemistry 38:3205–3210
11. Glenn JK, Morgan MA, Mayfield MB, Kuwahara M, Gold MH (1983) An extracellular H_2O_2-requiring enzyme preparation involved in lignin biodegradation by the white rot basidiomycete *Phanerochaete chrysosporium*. Biochem Biophys Res Commun 114:1077–1083
12. Chance B (1949) The reaction of catalase and cyanide. J Biol Chem 179:1299–1309
13. Niladevi KN (2009) In: Nigam PS, Pandey A (eds) Biotechnology for agro-industrial residues utilisation. Springer, Dordrecht, pp 397–414
14. Novotný Č et al (2004) Ligninolytic fungi in bioremediation: extracellular enzyme production and degradation rate. Soil Biol Biochem 36:1545–1551
15. Durán N, Esposito E (2000) Potential applications of oxidative enzymes and phenoloxidase-like compounds in wastewater and soil treatment: a review. Appl Catal B Environ 28:83–99
16. Regalado C, García-Almendárez BE, Duarte-Vázquez MA (2004) Biotechnological applications of peroxidases. Phytochem Rev 3:243–256
17. Choinowski T, Blodig W, Winterhalter KH, Piontek K (1999) The crystal structure of lignin peroxidase at 1.70 Å resolution reveals a hydroxy group on the Cβ of tryptophan 171: a novel radical site formed during the redox cycle1. J Mol Biol 286:809–827
18. Piontek K, Glumoff T, Winterhalter K (1993) Low pH crystal structure of glycosylated lignin peroxidase from *Phanerochaete chrysosporium* at 2.5 Å resolution. FEBS Lett 315:119–124
19. Edwards SL, Raag R, Wariishi H, Gold MH, Poulos TL (1993) Crystal structure of lignin peroxidase. Proc Natl Acad Sci USA 90:750–754
20. Poulos TL, Edwards SL, Wariishi H, Gold MH (1993) Crystallographic refinement of lignin peroxidase at 2 A. J Biol Chem 268:4429–4440
21. Schoemaker HE, Lundell TK, Hatakka AI, Piontek K (1994) The oxidation of veratryl alcohol, dimeric lignin models and lignin by lignin peroxidase: the redox cycle revisited. FEMS Microbiol Rev 13:321–331
22. Lundquist K, Kirk TK (1978) De novo synthesis and decomposition of veratryl alcohol by a lignindegrading basidiomycete. Phytochemistry 17:1676
23. Francesca Gerini M, Roccatano D, Baciocchi E, Nola AD (2003) Molecular dynamics simulations of lignin peroxidase in solution. Biophys J 84:3883–3893
24. Blodig W et al (1998) Autocatalytic formation of a hydroxy group at C beta of Trp171 in lignin peroxidase. Biochemistry 37:8832–8838
25. Doyle WA, Blodig W, Veitch NC, Piontek K, Smith AT (1998) Two substrate interaction sites in lignin peroxidase revealed by site-directed mutagenesis. Biochemistry 37:15097–15105
26. Timofeevski SL, Nie G, Reading NS, Aust SD (1999) Addition of veratryl alcohol oxidase activity to manganese peroxidase by site-directed mutagenesis. Biochem Biophys Res Commun 256:500–504
27. Sollewijn-Gelpke MD, Lee J, Gold MH (2002) Lignin peroxidase oxidation of veratryl alcohol: effects of the mutants H82A, Q222A, W171A, and F267L†. Biochemistry 41:3498–3506
28. Mester T et al (2001) Oxidation of a tetrameric nonphenolic lignin model compound by lignin peroxidase. J Biol Chem 276:22985–22990
29. Harvey PJ, Schoemaker HE, Palmer JM (1986) Veratryl alcohol as a mediator and the role of radical cations in lignin biodegradation by *Phanerochaete chrysosporium*. FEBS Lett 195:242–246
30. Goodwin DC, Aust SD, Grover TA (1995) Evidence for veratryl alcohol as a redox mediator in lignin peroxidase-catalyzed oxidation. Biochemistry 34:5060–5065
31. Candeias LP, Harvey PJ (1995) Lifetime and reactivity of the veratryl alcohol radical cation. Implications for lignin peroxidase catalysis. J Biol Chem 270:16745–16748
32. Baciocchi E, Bietti M, Francesca Gerini M, Lanzalunga O (2002) The mediation of veratryl alcohol in oxidations promoted by lignin peroxidase: the lifetime of veratryl alcohol radical cation. Biochem Biophys Res Commun 293:832–835
33. Khindaria A, Yamazaki I, Aust SD (1996) Stabilization of the veratryl alcohol cation radical by lignin peroxidase. Biochemistry 35:6418–6424
34. Khindaria A, Nie G, Aust SD (1997) Detection and characterization of the lignin peroxidase compound II-veratryl alcohol cation radical complex. Biochemistry 36:14181–14185
35. Johjima T et al (1999) Direct interaction of lignin and lignin peroxidase from *Phanerochaete chrysosporium*. Proc Natl Acad Sci USA 96:1989–1994
36. Baciocchi E, Fabbri C, Lanzalunga O (2003) Lignin peroxidase-catalyzed oxidation of nonphenolic trimeric lignin model compounds: fragmentation reactions in the intermediate radical cations. J Org Chem 68:9061–9069
37. Hammel KE, Moen MA (1991) Depolymerization of a synthetic lignin in vitro by lignin peroxidase. Enzyme Microb Technol 13:15–18
38. Paszczynski A, Crawford RL (1991) Degradation of azo compounds by ligninase from *Phanerochaete chrysosporium*:

involvement of veratryl alcohol. Biochem Biophys Res Commun 178:1056–1063
39. Chung N, Aust SD (1995) Veratryl alcohol-mediated indirect oxidation of phenol by lignin peroxidase. Arch Biochem Biophys 316:733–737
40. Huang X et al (2003) The roles of veratryl alcohol and nonionic surfactant in the oxidation of phenolic compounds by lignin peroxidase. Biochem Biophys Res Commun 311:491–494
41. Smith AT, Doyle WA (2006) Engineered peroxidases with veratryl alcohol oxidase activity. Patent (International). WO/2006-114616, 2 Nov 2006
42. Chen M et al (2011) Understanding lignin-degrading reactions of ligninolytic enzymes: binding affinity and interactional profile. PLoS One 6:e25647
43. Miki Y et al (2013) Formation of a tyrosine adduct involved in lignin degradation by *Trametopsis cervina* lignin peroxidase: a novel peroxidase activation mechanism. Biochem J 452:575–584
44. Miki Y, Ichinose H, Wariishi H (2010) Molecular characterization of lignin peroxidase from the white-rot basidiomycete *Trametes cervina*: a novel fungal peroxidase. FEMS Microbiol Lett 304:39–46
45. Miki Y et al (2011) Crystallographic, kinetic, and spectroscopic study of the first ligninolytic peroxidase presenting a catalytic tyrosine. J Biol Chem 286:15525–15534
46. Smith AT, Doyle WA, Dorlet P, Ivancich A (2009) Spectroscopic evidence for an engineered, catalytically active Trp radical that creates the unique reactivity of lignin peroxidase. Proc Natl Acad Sci 106:16084–16089
47. Bernini C, Pogni R, Basosi R, Sinicropi A (2012) The nature of tryptophan radicals involved in the long-range electron transfer of lignin peroxidase and lignin peroxidase-like systems: insights from quantum mechanical/molecular mechanics simulations. Proteins Struct Funct Bioinform 80:1476–1483
48. Piontek K, Smith AT, Blodig W (2001) Lignin peroxidase structure and function. Biochem Soc Trans 29:111–116
49. Berman HM et al (2000) The protein data bank. Nucleic Acids Res 28:235–242
50. Maestro (2014) Version 9.7, Schrödinger, LLC, New York, NY
51. Sastry GM, Adzhigirey M, Day T, Annabhimoju R, Sherman W (2013) Protein and ligand preparation: parameters, protocols, and influence on virtual screening enrichments. J Comput Aided Mol Des 27:221–234
52. Schrödinger Suite 2014-1 Protein Preparation Wizard
53. Blodig W, Smith AT, Doyle WA, Piontek K (2001) Crystal structures of pristine and oxidatively processed lignin peroxidase expressed in *Escherichia coli* and of the W171F variant that eliminates the redox active tryptophan 171. Implications for the reaction mechanism. J Mol Biol 305:851–861
54. Olsson MHM, Søndergaard CR, Rostkowski M, Jensen JH (2011) PROPKA3: consistent treatment of internal and surface residues in empirical pKa predictions. J Chem Theory Comput 7:525–537
55. Glide (2014) Version 6.2, Schrödinger, LLC, New York, NY
56. Friesner RA et al (2004) Glide: a new approach for rapid, accurate docking and scoring. 1. Method and assessment of docking accuracy. J Med Chem 47:1739–1749
57. Halgren TA et al (2004) Glide: a new approach for rapid, accurate docking and scoring. 2. Enrichment factors in database screening. J Med Chem 47:1750–1759
58. Banks JL et al (2005) Integrated modeling program, applied chemical theory (IMPACT). J Comput Chem 26:1752–1780
59. Desmond Molecular Dynamics System (2013) Version 3.4, D. E. Shaw Research, New York, NY
60. Berendsen HJC, Postma JPM, van Gunsteren WF, Hermans J (1981) In: Pullman B (ed) Intermolecular forces. Springer, Dordrecht, pp 331–342
61. Nosé S (1984) A unified formulation of the constant temperature molecular dynamics methods. J Chem Phys 81:511–519
62. Martyna GJ, Tobias DJ, Klein ML (1994) Constant pressure molecular dynamics algorithms. J Chem Phys 101:4177–4189
63. Essmann U et al (1995) A smooth particle mesh Ewald method. J Chem Phys 103:8577–8593
64. Tuckerman M, Berne BJ, Martyna GJ (1992) Reversible multiple time scale molecular dynamics. J Chem Phys 97:1990–2001
65. Prime (2014) Version 3.5, Schrödinger, LLC, New York, NY
66. Jacobson MP et al (2004) A hierarchical approach to all-atom protein loop prediction. Proteins Struct Funct Bioinform 55:351–367
67. Li J et al (2011) The VSGB 2.0 model: a next generation energy model for high resolution protein structure modeling. Proteins Struct Funct Bioinform 79:2794–2812
68. Mulakala C, Viswanadhan VN (2013) Could MM–GBSA be accurate enough for calculation of absolute protein/ligand binding free energies? J Mol Graph Model 46:41–51
69. Greenidge PA, Kramer C, Mozziconacci J-C, Wolf RM (2013) MM/GBSA binding energy prediction on the PDBbind data set: successes, failures, and directions for further improvement. J Chem Inf Model 53:201–209
70. MacroModel (2014) Version 10.3, Schrödinger, LLC, New York, NY
71. Shao J, Tanner SW, Thompson N, Cheatham TE (2007) Clustering molecular dynamics trajectories: 1. Characterizing the performance of different clustering algorithms. J Chem Theory Comput 3:2312–2334
72. Lama D et al (2013) Rational optimization of conformational effects induced by hydrocarbon staples in peptides and their binding interfaces. Sci Rep 3. doi:10.1038/srep03451
73. Hayes JM et al (2011) Kinetics, in silico docking, molecular dynamics, and MM–GBSA binding studies on prototype indirubins, KT5720, and staurosporine as phosphorylase kinase ATP-binding site inhibitors: the role of water molecules examined. Proteins 79:703–719
74. Takashima S et al (2007) Correlation between cellulose binding and activity of cellulose-binding domain mutants of *Humicola grisea* cellobiohydrolase 1. FEBS Lett 581:5891–5896
75. Linder M et al (1995) Identification of functionally important amino acids in the cellulose-binding domain of *Trichoderma reesei* cellobiohydrolase I. Protein Sci 4:1056–1064